Precipitation of niobium carbonitrides in ferrite: chemical composition measurements and thermodynamic modelling

M. PEREZ*†, E. COURTOIS†, D. ACEVEDO†, T. EPICIER† and P. MAUGIS‡

†GEMPPM, UMR CNRS 5510, 25 av. Capelle, N 69 621, Villeurbanne Cedex, France
‡ARCELOR Research SA, Voie Romaine, BP 30320, 57283 Maizières-lès-Metz, France

High-resolution transmission electron microscopy and electron-energy loss spectroscopy have been used to characterize the structure and chemical composition of niobium carbonitrides in the ferrite of a Fe–Nb–C–N model alloy at different precipitation stages. Experiments seem to indicate the coexistence of two types of precipitates: pure niobium nitrides and mixed sub-stoichiometric niobium carbonitrides. In order to understand the chemical composition of these precipitates, a thermodynamic formalism has been developed to evaluate the nucleation and growth rates (classical nucleation theory) and the chemical composition of nuclei and existing precipitates. A model based on the numerical solution of thermodynamic and kinetic equations is used to compute the evolution of the precipitate size distribution at a given temperature. The predicted compositions are in very good agreement with experimental results.

1. Introduction

Microalloyed steels have attracted considerable interest over many years and continue to gain wider industrial applications. A small addition of niobium to steel is known to yield significant improvements in its mechanical properties [1–3]. At high temperatures (1000–1300°C), niobium in solid solution retards austenite recrystallization and grain growth. At lower temperatures niobium combines with free carbon and nitrogen to form a fine dispersion of niobium carbide or carbonitride precipitates, which further inhibits austenite recovery and recrystallization prior to the γ/α transformation. The final effect is to increase the density of ferrite nucleation sites and thus reduce the final ferrite grain size. However, the detailed evolution of the precipitation in high-strength low alloy (HSLA) steels is still only partly understood.

*Corresponding author. Email: Michel.Perez@insa-lyon.fr

DOI: 10.1080/09500830701427003

For this reason, models have been developed in order to predict the influence of the process parameters on the state of precipitation. Precipitation models are generally based on the classical theory for diffusive phase transformation (see the review by Kampmann and Wagner [4]), and treat simultaneously the nucleation, growth and coarsening phenomena [5]. The particle size distribution, their number and volume fraction can be calculated [6–9].

Nevertheless, this theoretical approach needs to be compared with experimental data. Several TEM studies on HSLA have already been published [3, 10–13]. However, and owing to the previously mentioned difficulties, there is still a lack of comprehensive information of the evolution of the precipitation state as a function of annealing time and temperature: for example, no modelling of the precipitation kinetics, taking into account the chemistry of M-(C,N) precipitates, has been attempted.

This paper reports quantitative measurements of the chemical composition of the precipitate, and further focuses on the precipitation scenario that experimental results provide. A new thermodynamic formalism is presented and introduced in a model that gives a better understanding of the complex precipitation sequence observed experimentally.

2. Experimental

2.1. *Materials and sample preparation*

Table 1 shows the chemical composition of the investigated steel. The carbon and nitrogen contents were controlled such that the overall ratio of Nb to (C + N) was close to stoichiometry. The steel was heated to 1250°C for 20 min then water quenched to ensure complete dissolution of the precipitates. It has been established by TEM on both thin foils and extraction replicas that no undissolved precipitates were present after the quench. The steel was then subsequently annealed at 650°C. The annealing was carried out first in salt baths for short annealing times (5 and 30 min) and then under vacuum (quartz encapsulation) for longer annealing times (300 min and 126 h). After annealing, the specimens were water quenched.

TEM thin foils were obtained by the conventional method of careful grinding to produce a thin disc, followed by final thinning to electron transparency by electropolishing using a solution of 60% methanol – 35% butoxyethanol – 5% perchloric acid at −30°C [3].

Extraction replicas based on aluminium for carbon analysis were prepared by evaporating an amorphous alumina (AlO_x, $x < 3/2$) film onto a bulk sample

Table 1. Composition of our model steel (at. ppm).

Nb	C	N	S	Mn	Al	O	C/N	Nb/(C + N)
507	274	255	40	13	41	154	1.1	1.0

that had been polished and lightly pre-etched. Depositions were carried out as described by Scott *et al*. [14].

2.2. *Transmission electron microscopy and associated techniques*

Electron microscopy was performed using a JEOL 2010F field-emission-gun transmission electron microscope operating at 200 kV. The microscope was fitted with an Oxford EDX (energy-dispersive X-ray) analyzer and a Gatan DigiPEELS spectrometer, which uses a photodiode array detector for analysis by EELS (electron-energy-loss spectroscopy). The latter technique was employed to quantify the atomic ratio (C + N)/Nb for particles down to about 3 nm in radius. In order to avoid spurious signals from carbon contamination in the TEM, the alumina replicas were cooled to −170°C. A detailed description of the quantitative analysis of the precipitates by EELS can be found elsewhere [15, 16].

2.3. *Results*

In the earliest stages of precipitation (5 min at 650°C) it is possible to detect consistently precipitate nuclei using HRTEM, as illustrated in figure 1. Both monatomic platelets enriched in niobium and nitrogen and fcc carbonitrides

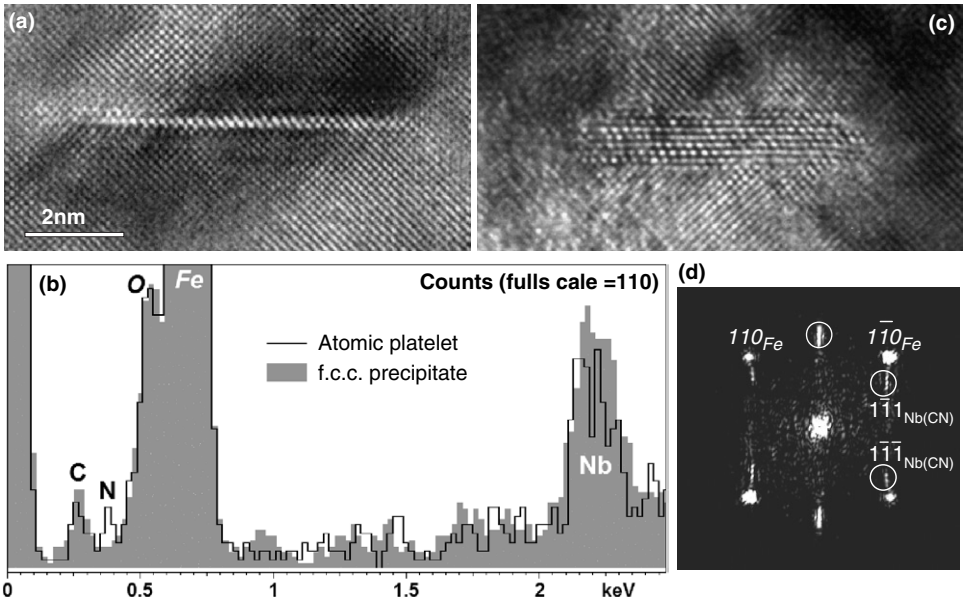

Figure 1. HRTEM images of $[100]_{Fe-\alpha}$ grains within a thin foil annealed for 5 min at 650°C: (a) monatomic platelet enriched in Nb; (b) EDX nanoanalysis (probe 2 nm) showing the Nb- and N-enrichment of the platelet (dark line) and the lower N-content within the precipitate shown in (c) (shaded spectrum); (c) NaCl-type structure of Nb(CN) nanoprecipitate seen along [110]. (d) Numerical diffractogram from (c) confirming the Baker–Nutting orientation relationship: $[001]_{Fe}//[110]_{Nb(CN)}$ (common azimuth) and $(200)_{Fe}//(002)_{Nb(CN)}$ (vertical reflection).

were detected. Both objects nucleate on {001} planes of the bcc ferrite lattice, the carbonitrides being in the expected Baker–Nutting orientation relationship with the matrix. The chemistry of these nuclei, difficult to ascertain in thin foils by TEM, has been confirmed by dedicated tomographic atom probe (TAP) measurements [15, 17].

For longer times (figure 2), both pure nitrides and carbonitrides have been observed, the chemistry of which has been unambiguously determined by EELS (according to the dedicated quantitative method described elsewhere [15, 16]), after annealing times of 30 min and 126 h. A previous experimental investigation

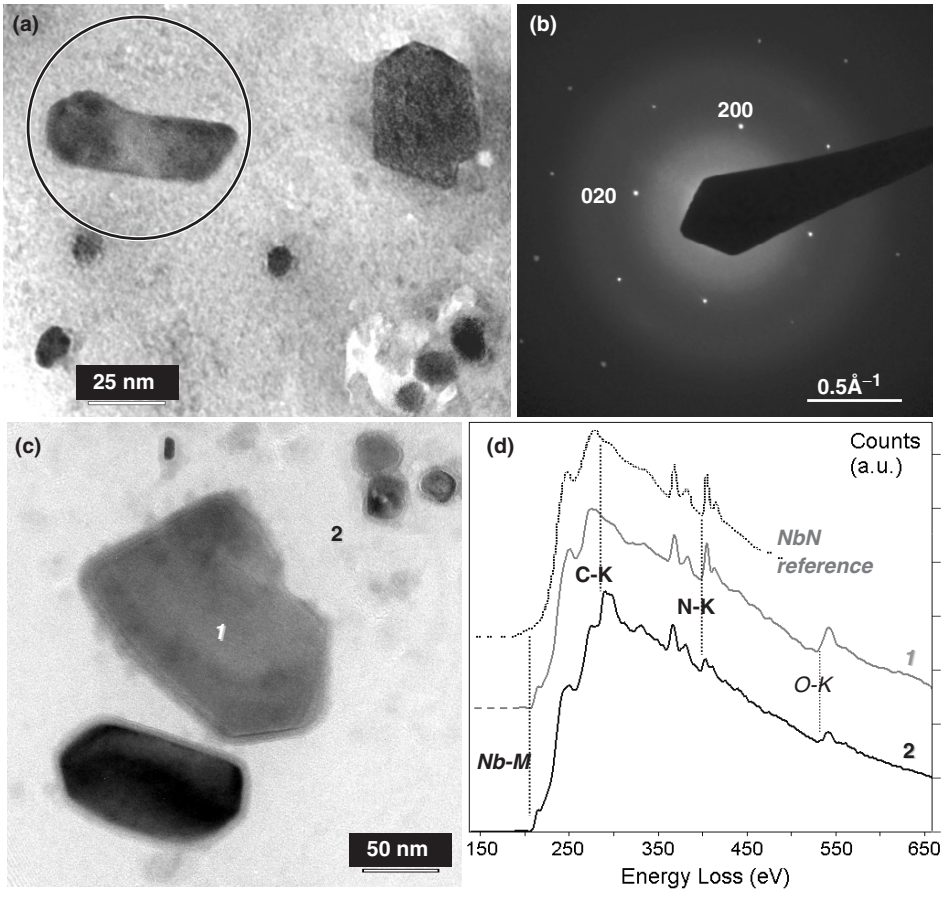

Figure 2. Precipitates observed from extraction replicas after treatments at 650°C: (a) bright-field TEM image after 30 min, showing large and smaller particles; (b) diffraction pattern of the precipitate circled in (a) (after a slight reorientation) consistent with the [001] zone axis of the NbN, NaCl-type structure ($a = 0.44$ nm); (c) same as (a) after 126 h, showing large and smaller particles (labelled 1 and 2, respectively). (d) EELS spectra from particles 1 and 2 showing that the large particles are pure niobium nitride [the EELS spectrum of a commercial powder of pure NbN (dotted curve) has been added for comparison], whereas the smaller ones are carbonitrides.

Table 2. EELS composition measurements (average of 35 analyses) of carbonitride precipitates. Results are given in atomic fraction ratios; the precision is ±0.05.

Temperature	Annealing time	(C + N)/Nb	C/Nb	C/(C + N)
650°C	30 min	0.85	0.58	0.68
650°C	126 h	0.87	0.52	0.59

suggests that a continuous solid solution exists between NbC and NbN [18], but, it is clearly found here that two populations of precipitates coexist simultaneously at 650°C: (i) pure and large stoichiometric nitrides NbN and (ii) complex smaller sub-stoichiometric carbonitrides NbC_xN_y. Electron diffraction shows that both types of particles have a cubic structure compatible with the expected fcc NaCl-type structure of Nb(CN) compounds (with $a = 0.440$ nm for pure NbN; see figure 2b), and $a = 0.447$ nm for pure NbC [15]). Results concerning the composition of carbonitrides are presented in table 2. They remain deficient in non-metal elements (C + N) even after annealing 126 h at 650°C, since the amount of interstitial species in precipitates is less than 90%. This finding is confirmed by TAP measurements performed on the same steel [17], which give a (C + N)/Nb ratio equal to 0.85 after 20 min annealing at 650°C. Moreover, complex carbonitrides contain more carbon than nitrogen. This could be interpreted as in contradiction with thermodynamics since nitrides are known to be much more stable than carbides [19]. This particular point will be discussed in the section on modelling.

From these experimental observations, a consistent precipitation scenario can be deduced, as illustrated in figure 3. The first stage of precipitation at 650°C (figure 3a) consists of the homogeneous nucleation of monatomic platelets, or 'GP' zones, which can be considered as the precursors of the future pure nitrides observed at longer annealing times. Simultaneously, slightly larger, although still nanometric in size, fcc-based nanoprecipitates develop, most probably heterogeneously (i.e. along dislocations), as currently observed in the case of pure niobium carbides in ferrite [3, 15, 20]. Further TEM observations on thin foils after 30 min at 650°C confirm unambiguously the homogenous and heterogeneous (i.e. on dislocations) precipitation of nitrides and carbonitrides, respectively [21]. A consistent thermodynamic modelling of the proposed scenario will be developed in the following section.

3. Thermodynamic modelling

In order to confirm and understand the previously derived scenario, a thermodynamic approach has been used. It is based on the two main observations:

(a) simultaneous precipitation of pure nitrides and complex carbonitrides;
(b) non-stoichiometry of carbonitrides: the presence of approx. 10% vacancies in the interstitial lattice.

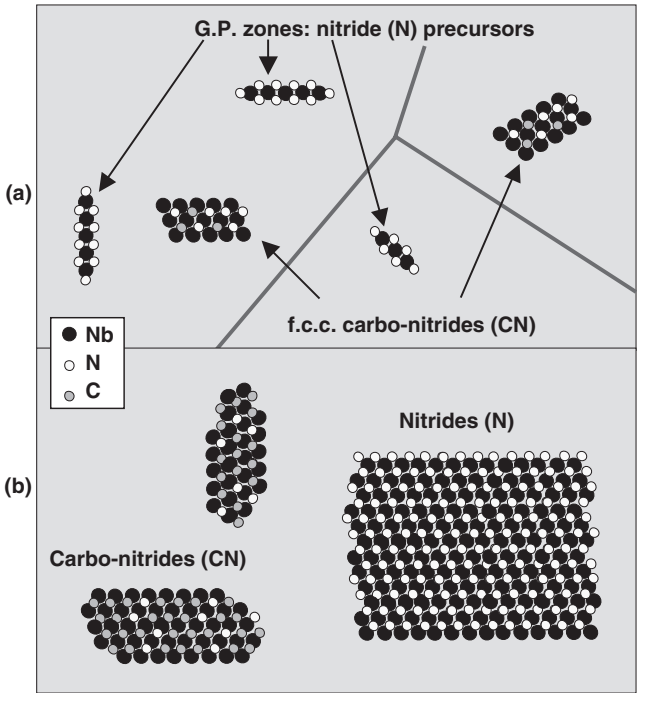

Figure 3. Scenario of precipitation deduced from the TEM and EELS analysis: (a) schematic microstructure at the early stage of precipitation; (b) same as (a) for longer annealing (see text for details).

The aim of this approach is to (i) describe the precipitation kinetics of both NbN and NbCN and (ii) predict the chemistry of complex carbonitrides NbCN, particularly the apparently contradictory C/N ratio.

A regular sublattice model [22], combined with classical nucleation theory and diffusion-controlled growth, has been used. Simultaneous precipitation of both phases has been performed using independent nucleation and growth rates for each phase (see Perez and Deschamps [8] for more details). The model has been implemented using dedicated precipitation software PreciSo. The thermodynamic calculations and their implementation will be described in detail in forthcoming papers [23, 24].

3.1. *Thermodynamics of complex carbonitrides*

Complex carbonitrides are assumed to be an ideal mixture of NbC and NbN_Z ($Z < 1$):

$$NbC_xN_y \leftrightarrow \chi NbC + (1-\chi)NbN_Z \quad \text{with } x = \chi \text{ and } y = (1-\chi)Z. \tag{1}$$

The parameter χ is the fraction of NbC molecules in the NbC_xN_y precipitate. The choice of mixing a stoichiometric carbide with a non-stoichiometric nitride has been

made in order to satisfy the global non-stoichiometry experimentally observed. Note that considering instead non-stoichiometric carbide and a stoichiometric nitride would have been an equivalent choice.

At equilibrium, two solubility products for NbC and NbN_Z can be defined: $K_{NbC} = X^e_{Nb}X^e_C/\chi$ and $K_{NbN_Z} = X^e_{Nb}X^{eZ}_N/(1-\chi)$, where X^e_{Nb}, X^e_C and X^e_N are the solute fractions in equilibrium with the precipitate. Assuming that the matrix is a regular diluted solution and that $Z \approx 1$, a first-order approximation gives $K_{NbN_Z} = K^Z_{NbN}$.

The driving force for nucleation, δg, and the nucleus composition, χ (the one that maximizes the driving force for nucleation $d(\delta g)/d\chi = 0$), are given by:

$$\delta g = \frac{kT}{v^P} S, S = \ln\left[\frac{(X_{Nb}X_C)^{\chi}\left(X_{Nb}X^z_N\right)^{(1-\chi)}}{[\chi K_{NbC}]^{\chi}\left[(1-\chi)K_{NbN_z}\right]^{(1-\chi)}}\right] \quad \text{and}$$

$$\chi^{-1} = 1 + \left[\frac{X_{Nb}X_C}{K_{NbC}}\right]^{-1}\left[\frac{X^z_{Nb}X_N}{K_{NbN_z}}\right], \tag{2}$$

where v^P is the volume of a molecule of NbC_xN_y, S is the matrix supersaturation and X_{Nb}, X_C, X_N are the Nb, C and N solute fractions, respectively.

Nucleation is derived from the classical theory [4], giving the nucleation rate:

$$\frac{dN}{dt} = N_0 Z^* \beta^* \exp\left[-\frac{\Delta G^*}{kT}\right]\left(1 - \exp\left[-\frac{t}{\tau}\right]\right),$$

$$\beta^* = \frac{4\pi R^{*2} D_{Nb} X_{Nb}}{a^4}, \quad R^* = \frac{R_0}{S}, \; R_0 = \frac{2\gamma v^P}{kT},$$

$$\Delta G^* = \frac{16\pi}{3}\frac{\gamma^3}{\delta g^2} = -\frac{\Delta G_0}{S^2}, \quad \Delta G_0 = \frac{4}{3}\pi R_0^2 \gamma, \; \tau = \frac{1}{2\beta^* Z^{*2}}$$

$$Z^* = \frac{v^P}{2\pi R^{*2}}\sqrt{\frac{R_0}{2v^P}}, \tag{3}$$

where N_0 is the number of nucleation sites ($N_0 = 1/a^3$ where a is the ferrite lattice parameter), Z^* is the Zeldovich factor, τ is the incubation time, R^* is the radius of the nucleus, γ is the surface energy of the interface matrix precipitate and D_{Nb} is the diffusion coefficient of niobium in ferrite.

Owing to the interface between matrix and precipitate, the equilibrium solute concentrations are modified. X^i_{Nb}, X^i_C and X^i_N are the new solute fractions in equilibrium with a precipitate of radius R. They are given by [9, 25]:

$$\exp\left(\frac{R_0}{R}\right) = \left(\frac{X^i_{Nb}X^i_C}{\chi K_{NbC}}\right) = \left(\frac{X^i_{Nb}X^i_N z}{(1-\chi)K_{NbNz}}\right). \tag{4}$$

The growth (shrinkage) of spherical particles is achieved by adding (removing) a shell of composition χ to existing particles, using the Fick equation in stationary regime. The growth rate is given by:

$$\frac{dR}{dt} = \frac{D_{Nb}}{R}\frac{X_{Nb} - X^i_{Nb}}{X^p_{Nb}\left(v^M_{at}/v^P_{at}\right) - X^i_{Nb}} = \frac{D_C}{R}\frac{X_C - X^i_C}{X^p_C\left(v^M_{at}/v^P_{at}\right) - X^i_C} = \frac{D_N}{R}\frac{X_N - X^i_N}{X^p_N\left(v^M_{at}/v^P_{at}\right) - X^i_N}, \tag{5}$$

where $X^P_{Nb} = 1/(1+x+y)$, $X^P_C = x/(1+x+y)$ and $X^P_N = y/(1+x+y)$, and D_C and D_N are the diffusion coefficients of carbon and nitrogen in ferrite. We have a set of five equations with five unknowns (dR/dt), X^i_N, X^i_C, X^i_{Nb} and χ, which can be solved numerically. Under the approximation D_N, $D_C \gg D_{Nb}$, it can be shown that χ is actually given by equation (2).

3.2. *Thermodynamics of pure nitrides*

The thermodynamics of pure nitrides is much simpler than that of carbonitrides: only one solubility product is involved. No equations are recalled here since they have all been presented in the preceding section. Pure NbN is a particular case where carbides are not considered ($\chi = 0$, $z = 1$).

3.3. *Simultaneous precipitation of pure NbN and complex NbCN*

The two populations of precipitates (pure NbN and complex NbC_xN_y) have their own nucleation and growth equations. Each family does not interact with the other, except when the mass balance is performed: at each time step, new solute concentrations are calculated taking into account the initial solute compositions, precipitates compositions and size distributions of both families.

3.4. *Precipitation software: PreciSo*

The thermodynamics presented in the preceding section have been implemented in the software PreciSo [23] (which is very similar to MultiPreci [9]), designed to predict precipitation kinetics (nucleation, growth and coarsening) for any kind of alloy. In this approach, the precipitate size distribution is modelled as follows: at each time step (time increment Δt), a new precipitate class is created [nucleation of a new class with radius R^* and number $(dN/dt)\,\Delta t$] and all existing classes with new radii are calculated: $R_i(t+\Delta t) = R_i(t) + (dR/dt|_i)\Delta t$. Note that, within this formalism, coarsening is implicitly taken into account thanks to the Gibbs–Thomson equation.

3.5. *Parameters*

Most of the parameters are taken from the literature as follows.

Diffusion coefficients: $D_{Nb} = 17 \times 10^{-4}$ [$m^2\,s^{-1}$]exp(−252 000 [$J\,mol^{-1}$]/RT), $D_N = 0.5 \times 10^{-6}$ [$m^2\,s^{-1}$]exp(−77 000[$J\,mol^{-1}$]/RT), $D_C = 0.62 \times 10^{-6}$[$m^2\,s^{-1}$] exp(−80 400[$J\,mol^{-1}$]/$RT$) [19].

Atomic volumes: $v_{NbN} = 1.04 \times 10^{-29}\,m^3$, $v_{NbCN} = 1.11 \times 10^{-29}\,m^3$) [19].

Solubility products: $\log_{10} K_{NbN} = 1.3396 - 12\,230/T$, $\log_{10} K_{NbC} = 1.8764 - 10960/T$ [26].

The coefficient giving the chemical composition and solubility product of NbN_Z has been adjusted in the range $Z \approx 1$ ($Z = 0.92$). Interfaces energies have also been adjusted to around 0.8 J m^{-2}, which is a reasonable value ($\gamma_{NbN} = 0.86\,J\,m^{-2}$ and $\gamma_{NbC_xN_y} = 0.78\,J\,m^{-2}$).

4. Results (after annealing at 650°C from 1 s to 10^7 s)

Figure 4 shows the transformed fraction of both populations: as observed experimentally, nitrides and carbonitrides precipitate simultaneously and coexist up to 10^7 s. The coexistence of both phases proves that they are both stable, i.e. their Gibbs energy is of the same order.

In figure 5, the solute fractions of niobium, carbon and nitrogen are plotted *versus* time. As expected, nitrogen is the first element to disappear since the nitride solubility product is very low. Once no nitrogen is left in solid solution, carbon becomes involved in precipitation.

The simulation results of figure 6 allow a better understanding of the complex precipitation sequence experimentally observed: while nitrogen is available in solid

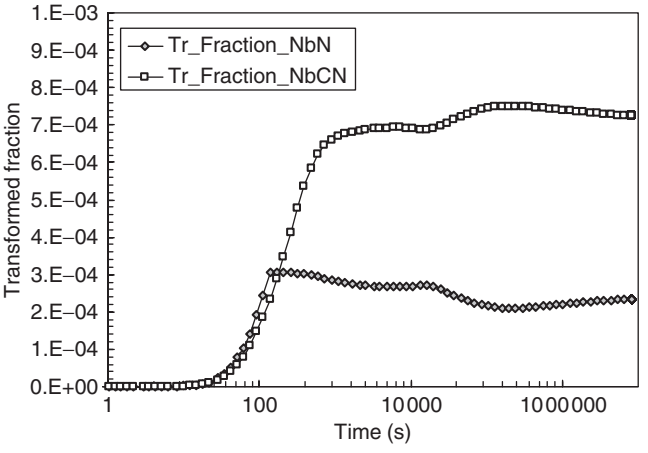

Figure 4. Precipitation kinetics: transformed fraction; nitrides and carbonitrides precipitate simultaneously.

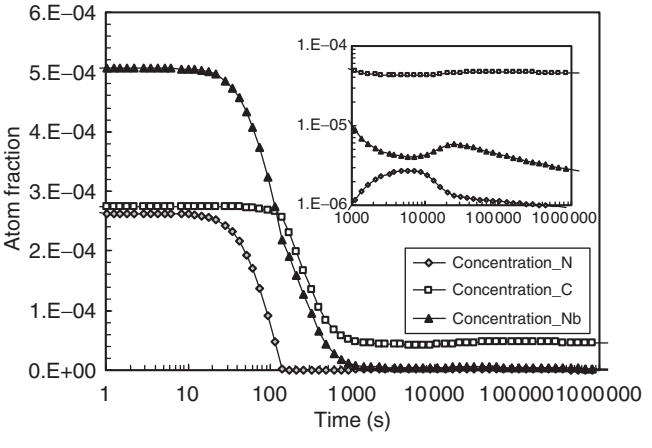

Figure 5. Precipitation kinetics: solute fraction; nitrogen is the first element to disappear.

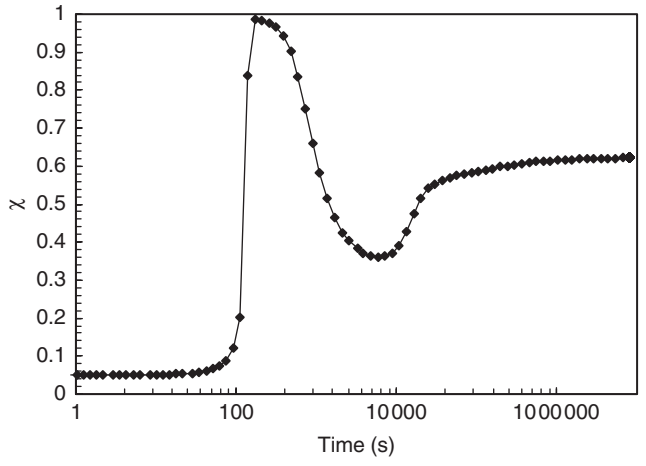

Figure 6. χ parameter: composition of nuclei and growth shells [see equation (1)]. Complex carbonitrides are nitrogen rich until no nitrogen is left in solid solution. The decrease of χ at 100 s and its increase at 10 000 s are related to the coarsening of NbN and NbCN, respectively (see Maugis and Perez [24] for more a detailed discussion). Finally, equilibrium is reached: carbon and nitrogen are redistributed in nitrides and carbonitrides.

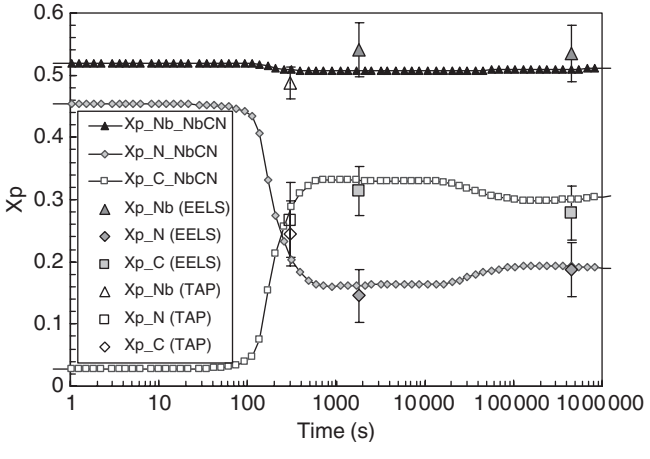

Figure 7. Chemical composition of carbonitrides. Very good agreement is obtained between chemical compositions measured by TAP [17] and EELS and the predicted composition obtained by the simulation.

solution, carbonitrides are mostly composed of nitrides ($\chi \approx 0.05$). But as soon as no nitrogen is left, carbonitrides become enriched in carbon. The decrease of χ at 100 s and its increase at 10↓000 s are related to the coarsening of NbN and NbCN, respectively (see elsewhere [24] for more a detailed discussion). Finally, equilibrium is reached: carbon and nitrogen are redistributed in nitrides and carbonitrides in order to equilibrate their chemical potentials.

Figure 7 shows the chemical composition of complex carbonitrides as a function of time. Very good agreement is observed between the EELS measurements and

the simulated results. Moreover, TAP measurements performed on the same samples [17] for shorter times are in perfect agreement with the simulation.

Hence, it is possible to interpret clearly the apparent contradiction concerning the evolution of the carbonitride C/N ratio: the nitrogen-rich carbonitrides are more stable and the pure nitride precipitates have absorbed a large part of the available nitrogen, leaving more carbon than nitrogen in the NbCN precipitates.

As it stands, the present model does not describe the heterogeneous nucleation of the carbonitride population, which could explain the larger numbers and smaller sizes of NbC_xN_y precipitates compared to nitrides (see figure 2). In order to improve the approach and provide quantitative results concerning the precipitate radius distribution and the precipitate density, the heterogeneous aspect of nucleation on dislocations should be taken into account in the model, as well as the non-spherical associated diffusion profile and precipitate shapes.

5. Conclusions

Fine precipitation of carbonitrides have been studied in a model steel, $FeNb_{(515\,ppm)}C_{(273\,ppm)}N_{(225\,ppm)}$. TEM, in association with EELS, has been applied to characterize the precipitation state for three different annealing times at 650°C. Precipitation of pure nitrides and complex non-stoichiometric carbon-rich carbonitrides occurs simultaneously.

A thermodynamic formalism for those precipitates has been proposed, leading to estimations of nucleation and growth rates, as well as precipitates compositions. A precipitation software (PreciSo) has been used to model the simultaneous precipitation of pure nitrides and complex carbonitrides.

Results are in very good agreements in terms of precipitate composition, allowing a better understanding of the complex precipitation sequence: (i) nitrides and niobium-rich carbonitrides precipitate, until no nitrogen is left; (ii) the chemical composition of the carbonitrides changes, incorporating more carbon; and (iii) an equilibrium is reached between the ferrite and both precipitates populations, NbN and $NbC_{0.59}N_{0.38}$.

Acknowledgments

Financial support from the French CPR-Precipitation (CNRS-CEA-Arcelor-Alcan) is gratefully acknowledged. Thanks are due to the CLYME (Consortium Lyonnais de Microscopie Électronique) in Lyon for access to the microscope and to the GPM (University of Rouen) for their willing collaboration in the context of the CPR-Precipitation.

References

[1] E.J. Palmiere, C.I. Garcia and A.J. Deardo, Metall. Mater. Trans. A **27** 951 (1996).
[2] C. Fossaert, G. Rees, T. Maurickx, *et al.*, Metall. Mater. Trans. A **26** 21 (1995).

[3] W.M. Rainforth, M.P. Black, R.L. Higginson, *et al*., Acta mater. **50** 735 (2002).
[4] R. Kampmann and R. Wagner, *Second-phase Precipitation in Materials Science and Technology: a Comprehensive Treatment*, Vol. 5 (VCH, Weinheim, 1991).
[5] H.R. Schercliff and M.F. Ashby, Acta Mater. **38** 1789 (1990).
[6] A. Deschamps and Y. Brechet, Acta Mater. **47** 293 (1999).
[7] O.R. Myhr and O. Grong, Acta Mater. **48** 1605 (2000).
[8] M. Perez and A. Deschamps, Mater. Sci. Engng A **360** 214 (2003).
[9] P. Maugis and M. Gouné, Acta Mater. **53** 3359 (2005).
[10] F. Hofer, P. Warbichler, B. Buchmayr, *et al*., J. Microsc. **184** 163 (1996).
[11] A.J. Craven, K. He, L.A. Gravie, *et al*., Acta Mater. **48** 3857 (2000).
[12] J.A. Wilson and A.J. Craven, Ultramicroscopy **94** 197 (2003).
[13] M. Beres, T.E. Weirich, K. Hulka, *et al*., Steel Res. Int. **75** 753 (2004).
[14] C.P. Scott, D. Charleix, P. Barges, *et al*., Scripta Mater. **47** 845 (2002).
[15] E. Courtois, PhD thesis, INSA-Lyon (2005).
[16] E. Courtois, T. Epicier and C. Scott, Micron **37** 492 (2006).
[17] F. Danoix, E. Bémont, P. Maugis, *et al*., Adv. Eng. Mat. **8** 1202 (2006).
[18] P. Villers, A. Prince and H. Okamoto (Editors), *Handbook of Ternary Alloy Phase Diagrams*, Vol. 6 (ASDM, Materials Park, OH, 1995) p. 7145.
[19] T. Gladmann, *The Physical Metallurgy of Microalloyed Steels* (Institute of Materials, London, 1997).
[20] F. Perrard, P. Donnadieu, A. Deschamps, *et al*., Phil. Mag. **86** 4271 (2006).
[21] T. Epicier, Adv. Eng. Mater. **8** 1197 (2006).
[22] M. Hillert and L.I. Staffansson, Acta Chem. Scand. **24** 3618 (1970).
[23] D. Acevedo and M. Perez, in preparation.
[24] P. Maugis and M. Perez, in preparation.
[25] M. Perez, Scripta Mater. **52** 709 (2005).
[26] R.C. Hudd, A. Jones and M.N. Kale, J. Iron Steel Inst. **209** 121 (1971).